Comparison of three-dimensional motion of bacteria with and without wall accumulation

Md Elius, Kenneth Boyle, Wei-Shun Chang, Pia H. Moisander, and Hangjian Ling

Phys. Rev. E **108**, 014409 — Published 28 July 2023

DOI: 10.1103/PhysRevE.108.014409

Comparison of 3D motion of bacteria with and without wall accumulation

Md Elius[1], Kenneth Boyle[2], Wei-Shun Chang[3], Pia H. Moisander[2], Hangjian Ling[1]*

[1] Department of Mechanical Engineering, University of Massachusetts Dartmouth, Dartmouth, MA, 02747
[2] Department of Biology, University of Massachusetts Dartmouth, Dartmouth, MA, 02747
[3] Department of Chemistry & Biochemistry, University of Massachusetts Dartmouth, Dartmouth, MA, 02747

*Corresponding: hling1@umassd.edu

Abstract: A comparison of the movement characteristics between bacteria with and without wall accumulation could potentially elucidate the mechanisms of biofilm formation. However, previous studies have mostly focused on the motion of bacteria that exhibit wall accumulation. Here, we applied digital holographic microscopy to compare the three-dimensional (3D) motions of two bacterial strains (*Shewanella japonica* UMDC19 and *Shewanella* sp. UMDC1): one exhibiting higher concentrations near the solid surfaces, and the other showing similar concentrations in near-wall and bulk regions. We found that the movement characteristics of the two strains are similar in the near-wall region, but are distinct in the bulk region. Near the wall, both strains have small velocities and mostly perform sub-diffusive motions. In the bulk, however, the bacteria exhibiting wall accumulation have significantly higher motility (including faster swimming speeds and longer movement trajectories) compared to the one showing no wall accumulation. Furthermore, we found that bacteria exhibiting wall accumulation slowly migrate from the bulk region to the near-wall region, and the hydrodynamic effect alone is insufficient to generate this migration speed. Future studies are required to test if the current findings apply to other bacterial species and strains.

Keywords: Wall accumulation; 3D bacterial motion; 3D tracking; digital holography;

Introduction

Numerous bacterial species show initial accumulation near solid surfaces prior to the formation of a biofilm [1], a matrix-enclosed bacterial population adherent to each other and/or to surfaces [2]. Biofilms impact human activities via issues such as marine biofouling [3]–[8], persistence of pathogenic infections [9]–[13], and food contamination [14]–[17], therefore, it is crucial to understand the mechanisms of biofilm formation and resilience. Wall accumulation of bacteria serves as an initial, important step to biofilm formation but the mechanisms are currently not well constrained. In the past several decades, the understanding of wall accumulation has been greatly improved by experimental and theoretical studies of bacterial movement near solid surfaces. Early microscopy imaging showed a strong increase of cell concentration near solid surfaces [18]–[20]. Later, three-dimensional bacterial tracking, by techniques such as digital holography microscopy [21]–[23], revealed that when approaching a wall, bacteria may reduce their swimming speed [24]–[26], switch to circular motion [27], [28], change body orientation [25], [27], [29], and reduce the tumble rate [26]. Furthermore, various theoretical models, based on disparate physical factors such as hydrodynamic interactions [30]–[33], Brownian motion [34]–[37], electrostatic and van der Waals interactions [18], [19], [38], or stochastic run-tumbling motions [39], [40], have been developed and successfully predicted the wall accumulation. For example, models based on hydrodynamic interactions showed that swimming microorganisms near a no-slip solid boundary creates a flow field that re-orientates and attracts cells to the wall [29], [41]. Recently, some studies have revealed that near-wall behaviors of bacteria and biofilm growth can be regulated by changing surface properties (e.g., surface stiffness)[42]–[48], by introducing flow shear [49]–[51] or an electric field [52]–[56].

Despite the extensive studies on the bacteria-wall interactions, previous studies mostly focused on the movement characteristics of bacteria that exhibit wall accumulation. Few studies directly compared the 3D movement of different bacterial species or strains that show different degrees of wall accumulation [57]. A

direct comparison of the movement statistic of bacteria with and without wall accumulation could provide insights into the mechanistic or behavioral processes proceeding biofilm formation. Here we employ digital holographic microscopy (DHM) and study the 3D movement of two *Shewanella* sp. strains: one showing higher density distribution near solid walls compared to the bulk region, and the other having similar density distribution in near wall and bulk regions. We analyze and compare the movement velocity and mean square displacement between the two bacterial species, and investigate which movement characteristics are correlated to the wall accumulation. In particular, we will test the hypothesis that bacteria exhibiting wall accumulation have larger swimming velocities and longer movement trajectories, according to previous studies which demonstrate the importance of motility on the biofilm formation [58]–[60]. Our results and approach are useful for the development and validation of new theoretical models for understanding the mechanisms of bacterial wall accumulation.

Material and Methods

The optical configuration of DHM for recording the growth and 3D motion of bacteria is shown in Fig. 1(a). A continuous He-Ne laser with a wavelength of λ=633 nm (Thorlab, model #HNL100RB, 10 mW) was used as a light source. The laser beam was attenuated by a neutral density filter, filtered by a spatial filter made up of a 25 μm pinhole and a 10× objective, and collimated into a 5 mm diameter before illuminating the bacterial sample. The bacterial sample was placed in a closed glass cuvette (FireflySci, lightpath 200 μm). The light scattered from the sample as well as the unscattered light were recorded by a CMOS camera (FLIR, model #GS3-U3-41C6M-C, 2048×2048 pixels, 5.5 μm pixel size). To achieve high magnification, a 10× objective (Edmund, model #46-144, infinity-corrected) and a 2× tube lens (Edmund, model #56-863, focal length 400 mm) were inserted before the camera. The calibrated magnification of the imaging system was 19.2×. By precisely translating the glass cuvette along the optical axis, the focal plane of the imaging system (i.e., hologram plane) was located at 30 μm away from the inner wall of the cuvette. Thus, all bacteria were located on one side of the hologram plane. We used a Cartesian coordinate system where x and y stand for the two in-plane directions and z for the out-of-plane direction. We defined z=0 at the inner wall of the glass container, and the bacterial cells are distributed at $0<z<200$ μm. The sample volume had a size of 590 μm × 590 μm × 200 μm (or 0.07 mm^3).

Two strains of marine bacteria *Shewanella* sp. (strains UMDC1 and UMDC19) were used in this study. The bacteria were originally isolated from marine biofilms in Northwestern Atlantic Ocean. For determining the 16S rRNA gene sequence, the culture were grown overnight, and the DNA was extracted using a phenol-chloroform method [61]. The amplification was conducted using 341F/785R primers [62], and the PCR conditions were as previously described [63]. The amplification products were cloned using pGEM-T in *E. coli* and sequenced at the Massachusetts General Hospital sequencing core. The primers were trimmed off from the sequences, and Blastn search was conducted on the NCBI database to identify the sequences. The best NCBI database matches for the strain UMDC1 were *Shewanella basaltis* and *S. ulleungensis* (99.77-100% nucleotide identity); here we refer to this strain as *Shewanella* sp., while the strain UMDC19 has a 100% nucleotide identity with *S. japonica*. Pairwise alignment of the 16S rRNA gene of UMDC1 and UMDC19 showed a nucleotide identity of 94.64%. Based on this dissimilarity, the two strains represent different species of the *Shewanella* genus. The 16S rRNA gene sequences are under NCBI accession numbers OQ034696-OQ034698.

To prepare the bacterial suspension for DHM experiments, a monoclonal culture was aseptically inoculated from a glycerol stock into sterile, 0.2 μm filtered Marine Broth (Difco Laboratories) and grown for 24h at 27°C in slow motion. The culture was diluted to a concentration where the optical density (OD) at 600 nm was approximately 0.05. The diluted bacterial suspension was then transferred into the glass cuvette for observations. We recorded data at 50 fps in the first 40 s at each hour, and ran the experiments for a duration of 4 hours. A total of 10,000 holograms were collected for each bacterial strain. The number of bacteria increased by 4 to 12 times during the 4-h experiments.

To calculate the 3D movement trajectories of bacteria from the recorded holograms, we used the following data analysis procedure. First, the background noise (e.g., signals from the dirt particles on glass windows and optical lenses) was removed by subtracting a background image obtained when there were no bacteria presented in the sample volume. The intensity distribution on the holograms after the background subtraction is denoted as I_H. Then, following previous work [64], [65], a 3D intensity field, denoted as $I(x, y, z)$, was reconstructed from the hologram by using the following equation:

$$I(x, y, z) = || [I_H - ||R||^2] \otimes h(x, y, z) ||, \quad (1)$$

where $||R||^2$ is the amplitude of the reference wave (here, $||R||^2$ is a constant since the reference wave is a plane wave), $h=z\exp\{ik(x^2+y^2+z^2)^{0.5}\}/[i\lambda(x^2+y^2+z^2)]$ is the Rayleigh–Sommerfeld diffraction kernel, $k=2\pi/\lambda$, and $\otimes$ represents a convolution. Since the intensity of the scattered light from the bacteria is much smaller compared to that of the reference light, we approximated $||R||^2$ using the average intensity of I_H. Figure 1(b) shows a sample hologram of one bacterium, and Figures 1(c-d) are the intensity distributions reconstructed from this hologram. Consistent to our previous work [64], [65] the bacterium appears to be an axially-elongated bright trace in the 3D intensity field reconstructed based on Eq. (1). The elongation in axial direction (i.e., z-direction) is known as the depth-of-focus issue in inline digital holography [66].

After obtaining the 3D intensity field, we detected the position of bacteria in 3D space following a 3D image segmentation technique used in our previous works [67], [68]. We first chose a global intensity threshold based on the intensities of the in-focus bacteria to discriminate between the background and the bacteria. Although a local threshold based on local standard deviation [69] could be used to improve the detection of cells with relatively low intensity, we found a global threshold was sufficient to detect more than 90% of the cells. After individual cell features were identified from the 3D volume, the cell position was calculated based on the intensity-weighted centroid of the 3D trace. Finally, we linked the 3D locations belonging to the same cell across different time frames based on a three-frame predictive particle tracking algorithm [70]. We applied a Gaussian smoothing and differentiating kernel [71] to the 3D trajectories to obtain accurate velocities and accelerations. The three velocity components were denoted as (u_x, u_y, u_z). For each bacterium, we also calculated the magnitude of the velocity component parallel to the wall as: $u_{//}=(u_x^2 + u_y^2)^{0.5}$. By definition, $u_{//}$ was always positive. The velocity component normal to the wall was u_z, which can be either positive or negative. Symbol <> was used to denote an ensemble average over all bacteria.

Figure 2 shows sample trajectories for UMDC1 and UMC19 obtained by the above data analysis procedure. The average observation time of cell trajectories was 2.7 s and 1.7 s for UMDC1 and UMDC19, respectively, much shorter than the observation time (40 s). This is partially because individual bacteria were not successfully detected at every frame. Due to the small size and nearly transparent nature of bacterial cells, the signal generated by bacteria on the holograms was very weak. As a result, detecting bacteria at every frame in DHM is a challenge, especially in a dense solution. One potential method to solve this challenge is by using dye to color the cells [72].

Results and Discussion

First, we examined the time-variation of the number of bacteria (i.e., growth of bacteria) in the sample volume. Figures 3(a-b) and 4(a-b) shows sample holograms at the beginning (t=0) and end (t=4 h) of the experiments for the two bacterial strains, UMDC1 and UMDC19, respectively. Clearly, for both species, the number of bacteria observed on the holograms increases over time, indicating the growth of bacterial populations via cell division. Figures 3(c) and 4(c) show the time-variations of number of bacteria obtained by processing the holograms. For both species, the number of bacteria in the 0.07 mm^3 sample volume remains nearly constant until the first two hours of the experiment and subsequently experiences an exponential increase. At t=4 h, the number of bacteria had increased by about 4 times for UMDC1 (from 90 to 360 cells), and 12 times for UMDC19 (from 40 to 500 cells). Based on the growth curves in Figures

3(c) and 4(c), we found a doubling time of 0.57 h and 0.70 h at the fast-growing stage (3 h<t<4 h) for UMDC19 and UMDC1, respectively.

We then analyzed the spatial distributions of the bacteria in the chamber to determine the presence of wall accumulation. Figures 3(d-e) and 4(d-e) show the spatial distribution of bacteria in the chamber at t=0 and 4 hours for the two species, respectively. Figures 3(f) and 4(f) show the histogram of the bacterial abundance with respect to distance from the wall at t=4 hours. Interestingly, for UMDC1, the densities of bacteria in the near-wall region and in the free-swimming region were very similar. In contrast, for UMDC19 at t=4 hours, the density of bacteria was much higher in the near-wall region than in the free-swimming region. The density of UMDC19 cells at t=3 hours (when the number of bacteria increased by same ratio compared to UMDC1 at t=4 hours) was also higher at the near-wall region compared to bulk region (see Supplemental Material, Fig. S1 [73]). Furthermore, as shown in Figure 5, we found the density distributions of UMDC19 has a good agreement with the model proposed by Berke *et al.* [29]. These results indicate that UMDC19 exhibits wall accumulation, while UMDC1 growth occurs uniformly across the entire chamber.

To understand which movement behavior contributes to the wall accumulation, we next analyzed the movement statistics. First, we compared the swimming velocities of the two bacterial species. Figures 6(a) and (b) plot the magnitudes of velocities in the direction parallel to the solid walls ($<u_{//}>$) and in the direction normal to the wall ($<|u_z|>$), respectively. Clearly, for both bacterial species, the magnitudes of $<u_{//}>$ and $<|u_z|>$ were on the same order, indicating that the bacterial motions were not confined in one particular direction. In the bulk region ($20<z<180$ μm), the magnitudes of $<u_{//}>$ and $<|u_z|>$ for bacteria with wall accumulation were much larger than these for the bacteria without wall accumulation (average swimming speed of 55 μm/s for UMDC19 vs. average swimming speed of 14 μm/s for UMDC1). This result suggests a correlation between wall accumulation and swimming speed, consistent with the previous studies which showed that bacteria with a higher motility are more likely to create biofilm [58]–[60]. However, our work did not prove a causal relationship between wall accumulation and swimming speed since the data were collected from two different bacterial strains. A future study comparing bacteria with and without movement pathways (such as flagellum synthesis) mutagenetically impaired will be informative in testing whether the wall accumulation is directly caused by large swimming velocity or whether other mechanisms are involved. Moreover, for bacteria with wall accumulation (UMDC19), both $<u_{//}>$ and $<|u_z|>$ significantly reduced when the cells approached the wall ($0<z<20$ μm and $180<z<200$ μm), indicating the wall entrapment. The reduction of bacterial swimming speed when approaching the wall is consistent to previous experimental [18], [20], [25] and theoretical [30] studies.

Figure 6(c) compares the velocity components normal to the solid walls ($<u_z>$) between the two bacterial species. Since u_z can be either positive or negative, once averaged over all bacteria, the magnitude of $<u_z>$ is much smaller compared to $<u_{//}>$ and $<|u_z|>$. For bacteria showing no wall accumulation (UMDC1), $<u_z>$ is nearly a constant zero across the entire chamber. However, for bacteria exhibiting wall accumulation (UMDC19), $<u_z>$ is negative on left-half of the chamber ($0<z<100$ μm) and positive on the right-half of the chamber ($100<z<200$ μm). The magnitude of $<u_z>$ has a maximum of 1.2 μm/s at about 20 μm away from the solid surfaces, and reduces to zero near the walls and the center of the chamber. This result indicates that there exists a long-range attraction force between the highly mobile bacteria and the solid walls. This attraction force might depend on or influence the swimming speed and appears bacterial strain specific: it is very weak for UMDC1 which swims slowly, and stronger for UMDC19 which swims faster. Moreover, this result implies that the wall accumulation is because of the migration of cells from the bulk region to the near-wall region, rather than faster cell growth in near-wall region.

To understand whether the long-range attraction between UMDC19 and solid walls is originated from the hydrodynamic interaction, we next calculate the hydrodynamically induced wall-normal velocity u_z by a cell moving parallel to a no-slip solid wall as [29]:

$$u_z = -\frac{3p}{64\pi\mu}\left(\frac{1}{z^2} - \frac{1}{(H-z)^2}\right) \quad (2)$$

where p is the force dipole strength (the cell is approximated as a force dipole), μ is the viscosity of the liquid, and H is the distance between two parallel walls. The force dipole is on the order of the drag force times the cell size, $p \sim \mu U L^2$, where L is the cell size and U is the swimming speed. For UMDC19, we estimate p=1.4 *pN μm*, by assuming $\mu = 1\times10^{-3}$ *kg/m/s* (viscosity of water), U=55 *μm/s* and L=5 *μm*. Figure 6(c) also plots u_z predicted by Equ. (2) with p=1.4 *pN μm*. The result shows that in the bulk region the velocity induced by the hydrodynamic interactions is much smaller than the observed velocity for UMDC19. Therefore, in addition to the hydrodynamic effect, there are other mechanisms (e.g., the stochastic run-tumbling behavior) that drive the cells to migrate from the bulk region to the near-wall region. Further studies are required to understand which mechanisms contribute to this large migration speed.

To further seek evidence on cell migration from the bulk region to the near-wall regions, we plotted the time-variations of z-position for a few bacteria UMDC19, as shown in Figure 7. Clearly, some bacteria initially located in the bulk region (50 μm<z<150 μm) migrated to one of the walls at z=0 and z=200 μm, and remained on the walls for more than 2 s.

Lastly, we compared the 3D movement trajectories of the two strains of bacteria in the bulk (50<z<150 μm) and near-wall (0<z<10 μm and 190<z<200 μm) regions. We classified the trajectories by first calculating the mean-square-displacement (Δr^2) and then fitting Δr^2 with respect to time lag (Δt) as $\Delta r^2 = \alpha \Delta t^K$, where K is the power exponent and α is a constant. Based on the measured value of K, the trajectories were divided into two categories: sub-diffusive (or in-active) motion for K<1, and super-diffusive (or active) motion for K>1. Note, to obtain meaningful K, we only selected the trajectories whose length was longer than 1 s for analysis. Changing this minimal length requirement from 1 s to 2 s did not alter the conclusion (see Supplemental Material, Fig. S2 [73]). In addition, we calculated Δr^2 based on the bacterial displacements in x and y directions, instead of the bacterial displacements in all three directions. The reason is that the measurement uncertainty of z position of bacteria is relatively larger than that in x and y directions, due to the inherent limitation of digital holography [65]. A comparison of Δr^2 based on bacterial displacement in all three directions and bacterial displacement in x and y directions can be found in Supplemental Material, Fig. S3 [73]. Sample profiles of Δr^2 based on the bacterial displacements in x and y directions and power-law fittings can be found in Supplemental Material, Fig. S4 [73].

Figures 8(a) and (b) show sample bacteria trajectories in the bulk region for UMDC1 and UMDC19, respectively. Figure 8(c) shows the probability density distributions of K in the bulk region. Clearly, for bacteria exhibiting wall accumulation (UMDC19), K has a peak value close to K=2. However, for bacteria showing no wall accumulation (UMDC1), K has two peaks located near K=1 and K=2 respectively. This result further indicates that bacteria exhibiting wall accumulation have a higher motility. Figures 8(d) and (e) show sample bacteria trajectories in the near-wall region for UMDC1 and UMDC19, respectively. Figure 8(f) shows the probability density distributions of K in the near-wall region. For both bacterial strains, the percentages of trajectories showing sub-diffusive motions were about 50%, larger than these in the bulk region. The increase of sub-diffusive motions in near-wall regions is mainly due to the constrain of solid walls, consistent to previous studies [24]–[26].

Conclusion

In summary, by using digital holographic microscopy, we tracked and compared the three-dimensional motions of two bacterial species of the same genus (*Shewanella* sp. UMDC1 and *Shewanella japonica* UMDC19). UMDC19 had higher density distribution near the walls, while UMDC1 showed similar density distributions in the near-wall and the bulk regions. We found that the bacteria exhibiting wall accumulation have much higher motility compared to the ones showing no wall accumulation. The high motility presents

in the forms of greater swimming speeds and distinct super-diffusive trajectories. Furthermore, we found that bacteria exhibiting wall accumulation slowly migrate from the bulk region to the near-wall region, with a velocity normal to the surface reaching to a maximum of 1.2 μm/s at 20 μm away from the walls. This result suggests the existence of a long-range attraction force between the bacteria and the solid surface, and that the wall accumulation is due to the migration of cells from bulk region to near-wall region. We also found that the hydrodynamic interaction alone is insufficient to produce the migration speed, suggesting the migration is due to active bacterial movement toward the inert surface. Future studies are required to explain the origin of the long-range attraction force and the migration speed.

The current study only considered two different bacterial strains. Future works are required to test if our results can be generally applied to other bacterial species. In particular, our work only showed a correlation not a causal relation between wall accumulation and motility. To prove the impact of motility on wall accumulation, future work is required to compare the 3D motion of the same bacteria with and without motility. Nevertheless, holographic microscopy as demonstrated here is a powerful tool in describing bacterial swimming behavior and speed, as well as wall accumulation.

Data accessibility
We provide 10 movies showing sample holograms for two bacterial species UMDC1 and UMDC19, 5 for each recorded at every 1 hour. We also provide 10 MATLAB data files that include the 3D tracking results corresponding to the recorded holograms for two bacterial species and 5 time steps. These movies and datafiles are available at figshare: https://figshare.com/s/c9ef39ac6e9a85c4cd0b. The bacterial strains are available from the authors upon request.

Competing interests
We declare we have no competing interests.

Authors' contributions
H.L., P.H.M., and W.S.C. designed the methodology; M.E., K.B., and H.L. collected the data; M.E. and H.L. analyzed the data and led the writing of the manuscript. All authors contributed critically to the drafts and gave final approval for publication.

Acknowledgement
We thank Abhishek Naik for isolating the UMDC1 strain.

Funding
UMass Dartmouth's Marine and Undersea Technology (MUST) Research Program funded by the Office of Naval Research (ONR) under Grant No. N00014-20-1-2170.

References
[1] H.-C. Flemming and S. Wuertz, "Bacteria and archaea on Earth and their abundance in biofilms," *Nat Rev Microbiol*, vol. 17, no. 4, Art. no. 4, Apr. 2019, doi: 10.1038/s41579-019-0158-9.
[2] J. W. Costerton, Z. Lewandowski, D. E. Caldwell, D. R. Korber, and H. M. Lappin-Scott, "Microbial biofilms," *Annual Review of Microbiology*, vol. 49, pp. 711–747, Jan. 1995.
[3] M. Callow and J. E. Callow, "Marine biofouling: a sticky problem.," *Biologist*, 2002.
[4] J. Bannister, M. Sievers, F. Bush, and N. Bloecher, "Biofouling in marine aquaculture: a review of recent research and developments," *Biofouling*, vol. 35, no. 6, pp. 631–648, Jul. 2019, doi: 10.1080/08927014.2019.1640214.
[5] R. Venkatesan, J. Kadiyam, P. SenthilKumar, R. Lavanya, and L. Vedaprakash, "Marine Biofouling on Moored Buoys and Sensors in the Northern Indian Ocean," *Marine Technology Society Journal*, vol. 51, no. 2, pp. 22–30, Mar. 2017, doi: 10.4031/MTSJ.51.2.11.

[6] P. Priyanka, A. B. Arun, C. C. Young, and P. D. Rekha, “Prospecting exopolysaccharides produced by selected bacteria associated with marine organisms for biotechnological applications,” *Chin J Polym Sci*, vol. 33, no. 2, pp. 236–244, Feb. 2015, doi: 10.1007/s10118-015-1581-7.
[7] I. Fitridge, T. Dempster, J. Guenther, and R. de Nys, “The impact and control of biofouling in marine aquaculture: a review,” *Biofouling*, vol. 28, no. 7, pp. 649–669, Aug. 2012, doi: 10.1080/08927014.2012.700478.
[8] K. E. Cooksey and B. Wigglesworth-Cooksey, “Adhesion of bacteria and diatoms to surfaces in the sea: a review,” *Aquatic Microbial Ecology*, Jan. 1995, doi: 10.3354/ame009087.
[9] J. W. Costerton, P. S. Stewart, and E. P. Greenberg, “Bacterial Biofilms: A Common Cause of Persistent Infections,” *Science*, vol. 284, no. 5418, pp. 1318–1322, May 1999, doi: 10.1126/science.284.5418.1318.
[10] Z. Khatoon, C. D. McTiernan, E. J. Suuronen, T.-F. Mah, and E. I. Alarcon, “Bacterial biofilm formation on implantable devices and approaches to its treatment and prevention,” *Heliyon*, vol. 4, no. 12, p. e01067, Dec. 2018, doi: 10.1016/j.heliyon.2018.e01067.
[11] M. Habash and G. Reid, “Microbial Biofilms: Their Development and Significance for Medical Device—Related Infections,” *The Journal of Clinical Pharmacology*, vol. 39, no. 9, pp. 887–898, 1999, doi: 10.1177/00912709922008506.
[12] M. M. Mihai *et al.*, “Microbial biofilms: impact on the pathogenesis of periodontitis, cystic fibrosis, chronic wounds and medical device-related infections,” *Curr Top Med Chem*, vol. 15, no. 16, pp. 1552–1576, 2015, doi: 10.2174/1568026615666150414123800.
[13] S. Häussler and M. R. Parsek, “Biofilms 2009: New Perspectives at the Heart of Surface-Associated Microbial Communities,” *Journal of Bacteriology*, vol. 192, no. 12, pp. 2941–2949, Jun. 2010, doi: 10.1128/JB.00332-10.
[14] J. Miao *et al.*, “Formation and development of Staphylococcus biofilm: With focus on food safety,” *Journal of Food Safety*, vol. 37, no. 4, p. e12358, 2017, doi: 10.1111/jfs.12358.
[15] C. Darby, J. W. Hsu, N. Ghori, and S. Falkow, “Plague bacteria biofilm blocks food intake,” *Nature*, vol. 417, no. 6886, Art. no. 6886, May 2002, doi: 10.1038/417243a.
[16] K. Myszka and K. Czaczyk, “Bacterial Biofilms on Food Contact Surfaces - a Review,” *Pol. J. Food Nutr. Sci.*, vol. 61, no. 3, pp. 173–180, Sep. 2011, doi: 10.2478/v10222-011-0018-4.
[17] G. M. Abebe, “The Role of Bacterial Biofilm in Antibiotic Resistance and Food Contamination,” *International Journal of Microbiology*, vol. 2020, p. e1705814, Aug. 2020, doi: 10.1155/2020/1705814.
[18] P. D. Frymier, R. M. Ford, H. C. Berg, and P. T. Cummings, “Three-dimensional tracking of motile bacteria near a solid planar surface,” *Proc Natl Acad Sci U S A*, vol. 92, no. 13, pp. 6195–6199, Jun. 1995, doi: 10.1073/pnas.92.13.6195.
[19] M. A. Vigeant and R. M. Ford, “Interactions between motile Escherichia coli and glass in media with various ionic strengths, as observed with a three-dimensional-tracking microscope,” *Appl Environ Microbiol*, vol. 63, no. 9, pp. 3474–3479, Sep. 1997, doi: 10.1128/aem.63.9.3474-3479.1997.
[20] P. D. Frymier and R. M. Ford, “Analysis of bacterial swimming speed approaching a solid–liquid interface,” *AIChE Journal*, vol. 43, no. 5, pp. 1341–1347, 1997, doi: 10.1002/aic.690430523.
[21] S. Bianchi, F. Saglimbeni, G. Frangipane, D. Dell’Arciprete, and R. D. Leonardo, “3D dynamics of bacteria wall entrapment at a water–air interface,” *Soft Matter*, vol. 15, no. 16, pp. 3397–3406, Apr. 2019, doi: 10.1039/C9SM00077A.
[22] S. M. Vater *et al.*, “Swimming Behavior of Pseudomonas aeruginosa Studied by Holographic 3D Tracking,” *PLOS ONE*, vol. 9, no. 1, p. e87765, Jan. 2014, doi: 10.1371/journal.pone.0087765.
[23] M. Heydt *et al.*, “Settlement behavior of zoospores of Ulva linza during surface selection studied by digital holographic microscopy,” *Biointerphases*, vol. 7, no. 1–4, p. 33, Dec. 2012, doi: 10.1007/s13758-012-0033-y.

[24] M. Qi, X. Gong, B. Wu, and G. Zhang, “Landing Dynamics of Swimming Bacteria on a Polymeric Surface: Effect of Surface Properties,” *Langmuir*, vol. 33, no. 14, pp. 3525–3533, Apr. 2017, doi: 10.1021/acs.langmuir.7b00439.
[25] S. Bianchi, F. Saglimbeni, and R. Di Leonardo, “Holographic Imaging Reveals the Mechanism of Wall Entrapment in Swimming Bacteria,” *Phys. Rev. X*, vol. 7, no. 1, p. 011010, Jan. 2017, doi: 10.1103/PhysRevX.7.011010.
[26] M. Molaei, M. Barry, R. Stocker, and J. Sheng, “Failed escape: solid surfaces prevent tumbling of Escherichia coli,” *Phys Rev Lett*, vol. 113, no. 6, p. 068103, Aug. 2014, doi: 10.1103/PhysRevLett.113.068103.
[27] E. Lauga, W. R. DiLuzio, G. M. Whitesides, and H. A. Stone, “Swimming in Circles: Motion of Bacteria near Solid Boundaries,” *Biophysical Journal*, vol. 90, no. 2, pp. 400–412, Jan. 2006, doi: 10.1529/biophysj.105.069401.
[28] R. Di Leonardo, D. Dell’Arciprete, L. Angelani, and V. Iebba, “Swimming with an Image,” *Phys. Rev. Lett.*, vol. 106, no. 3, p. 038101, Jan. 2011, doi: 10.1103/PhysRevLett.106.038101.
[29] A. P. Berke, L. Turner, H. C. Berg, and E. Lauga, “Hydrodynamic Attraction of Swimming Microorganisms by Surfaces,” *Phys. Rev. Lett.*, vol. 101, no. 3, p. 038102, Jul. 2008, doi: 10.1103/PhysRevLett.101.038102.
[30] M. Ramia, D. L. Tullock, and N. Phan-Thien, “The role of hydrodynamic interaction in the locomotion of microorganisms,” *Biophysical Journal*, vol. 65, no. 2, pp. 755–778, Aug. 1993, doi: 10.1016/S0006-3495(93)81129-9.
[31] D. Giacché, T. Ishikawa, and T. Yamaguchi, “Hydrodynamic entrapment of bacteria swimming near a solid surface,” *Phys. Rev. E*, vol. 82, no. 5, p. 056309, Nov. 2010, doi: 10.1103/PhysRevE.82.056309.
[32] G.-J. Li and A. M. Ardekani, “Hydrodynamic interaction of microswimmers near a wall,” *Phys. Rev. E*, vol. 90, no. 1, p. 013010, Jul. 2014, doi: 10.1103/PhysRevE.90.013010.
[33] K. Schaar, A. Zöttl, and H. Stark, “Detention Times of Microswimmers Close to Surfaces: Influence of Hydrodynamic Interactions and Noise,” *Phys. Rev. Lett.*, vol. 115, no. 3, p. 038101, Jul. 2015, doi: 10.1103/PhysRevLett.115.038101.
[34] G. Li, L.-K. Tam, and J. X. Tang, “Amplified effect of Brownian motion in bacterial near-surface swimming,” *Proceedings of the National Academy of Sciences*, vol. 105, no. 47, pp. 18355–18359, Nov. 2008, doi: 10.1073/pnas.0807305105.
[35] G. Li and J. X. Tang, “Accumulation of Microswimmers near a Surface Mediated by Collision and Rotational Brownian Motion,” *Phys. Rev. Lett.*, vol. 103, no. 7, p. 078101, Aug. 2009, doi: 10.1103/PhysRevLett.103.078101.
[36] G. Li *et al.*, “Accumulation of swimming bacteria near a solid surface,” *Phys. Rev. E*, vol. 84, no. 4, p. 041932, Oct. 2011, doi: 10.1103/PhysRevE.84.041932.
[37] A. Ahmadzadegan, S. Wang, P. P. Vlachos, and A. M. Ardekani, “Hydrodynamic attraction of bacteria to gas and liquid interfaces,” *Phys. Rev. E*, vol. 100, no. 6, p. 062605, Dec. 2019, doi: 10.1103/PhysRevE.100.062605.
[38] M. A.-S. Vigeant, R. M. Ford, M. Wagner, and L. K. Tamm, “Reversible and irreversible adhesion of motile Escherichia coli cells analyzed by total internal reflection aqueous fluorescence microscopy,” *Appl Environ Microbiol*, vol. 68, no. 6, pp. 2794–2801, Jun. 2002, doi: 10.1128/AEM.68.6.2794-2801.2002.
[39] B. Ezhilan, R. Alonso-Matilla, and D. Saintillan, “On the distribution and swim pressure of run-and-tumble particles in confinement,” *Journal of Fluid Mechanics*, vol. 781, p. R4, Oct. 2015, doi: 10.1017/jfm.2015.520.
[40] J. Elgeti and G. Gompper, “Run-and-tumble dynamics of self-propelled particles in confinement,” *EPL*, vol. 109, no. 5, p. 58003, Mar. 2015, doi: 10.1209/0295-5075/109/58003.

[41] K. Drescher, J. Dunkel, L. H. Cisneros, S. Ganguly, and R. E. Goldstein, “Fluid dynamics and noise in bacterial cell–cell and cell–surface scattering,” *Proceedings of the National Academy of Sciences*, vol. 108, no. 27, pp. 10940–10945, Jul. 2011, doi: 10.1073/pnas.1019079108.
[42] M. Qi, Q. Song, J. Zhao, C. Ma, G. Zhang, and X. Gong, “Three-Dimensional Bacterial Behavior near Dynamic Surfaces Formed by Degradable Polymers,” *Langmuir*, vol. 33, no. 45, pp. 13098–13104, Nov. 2017, doi: 10.1021/acs.langmuir.7b02806.
[43] Q. Peng *et al.*, “Three-Dimensional Bacterial Motions near a Surface Investigated by Digital Holographic Microscopy: Effect of Surface Stiffness,” *Langmuir*, vol. 35, no. 37, pp. 12257–12263, Sep. 2019, doi: 10.1021/acs.langmuir.9b02103.
[44] D. Campoccia, L. Montanaro, and C. R. Arciola, “A review of the biomaterials technologies for infection-resistant surfaces,” *Biomaterials*, vol. 34, no. 34, pp. 8533–8554, Nov. 2013, doi: 10.1016/j.biomaterials.2013.07.089.
[45] L. C. Hsu, J. Fang, D. A. Borca-Tasciuc, R. W. Worobo, and C. I. Moraru, “Effect of Micro- and Nanoscale Topography on the Adhesion of Bacterial Cells to Solid Surfaces,” *Appl Environ Microbiol*, vol. 79, no. 8, pp. 2703–2712, Apr. 2013, doi: 10.1128/AEM.03436-12.
[46] C. Díaz, P. L. Schilardi, R. C. Salvarezza, and M. Fernández Lorenzo de Mele, “Have flagella a preferred orientation during early stages of biofilm formation?: AFM study using patterned substrates,” *Colloids Surf B Biointerfaces*, vol. 82, no. 2, pp. 536–542, Feb. 2011, doi: 10.1016/j.colsurfb.2010.10.013.
[47] F. Song, M. E. Brasch, H. Wang, J. H. Henderson, K. Sauer, and D. Ren, “How Bacteria Respond to Material Stiffness during Attachment: A Role of Escherichia coli Flagellar Motility,” *ACS Appl Mater Interfaces*, vol. 9, no. 27, pp. 22176–22184, Jul. 2017, doi: 10.1021/acsami.7b04757.
[48] F. Song and D. Ren, “Stiffness of cross-linked poly(dimethylsiloxane) affects bacterial adhesion and antibiotic susceptibility of attached cells,” *Langmuir*, vol. 30, no. 34, pp. 10354–10362, Sep. 2014, doi: 10.1021/la502029f.
[49] M. Molaei and J. Sheng, “Succeed escape: Flow shear promotes tumbling of Escherichia colinear a solid surface,” *Sci Rep*, vol. 6, no. 1, Art. no. 1, Oct. 2016, doi: 10.1038/srep35290.
[50] A. Chengala, M. Hondzo, and J. Sheng, “Microalga propels along vorticity direction in a shear flow,” *Phys. Rev. E*, vol. 87, no. 5, p. 052704, May 2013, doi: 10.1103/PhysRevE.87.052704.
[51] J. T. Locsei and T. J. Pedley, “Run and tumble chemotaxis in a shear flow: the effect of temporal comparisons, persistence, rotational diffusion, and cell shape,” *Bull Math Biol*, vol. 71, no. 5, pp. 1089–1116, Jul. 2009, doi: 10.1007/s11538-009-9395-9.
[52] H. Kang, S. Shim, S. J. Lee, J. Yoon, and K. H. Ahn, “Bacterial translational motion on the electrode surface under anodic electric field,” *Environ Sci Technol*, vol. 45, no. 13, pp. 5769–5774, Jul. 2011, doi: 10.1021/es200752h.
[53] T.-K. Lim, T. Murakami, M. Tsuboi, K. Yamashita, and T. Matsunaga, “Preparation of a colored conductive paint electrode for electrochemical inactivation of bacteria,” *Biotechnol Bioeng*, vol. 81, no. 3, pp. 299–304, Feb. 2003, doi: 10.1002/bit.10469.
[54] A. J. van der Borden *et al.*, “Prevention of pin tract infection in external stainless steel fixator frames using electric current in a goat model,” *Biomaterials*, vol. 28, no. 12, pp. 2122–2126, Apr. 2007, doi: 10.1016/j.biomaterials.2007.01.001.
[55] A. J. van der Borden, H. C. van der Mei, and H. J. Busscher, “Electric-current-induced detachment of Staphylococcus epidermidis strains from surgical stainless steel,” *J Biomed Mater Res B Appl Biomater*, vol. 68, no. 2, pp. 160–164, Feb. 2004, doi: 10.1002/jbm.b.20015.
[56] S. H. Hong *et al.*, “Effect of electric currents on bacterial detachment and inactivation,” *Biotechnol Bioeng*, vol. 100, no. 2, pp. 379–386, Jun. 2008, doi: 10.1002/bit.21760.

[57] A. L. Hook *et al.*, “Simultaneous Tracking of Pseudomonas aeruginosa Motility in Liquid and at the Solid-Liquid Interface Reveals Differential Roles for the Flagellar Stators,” *mSystems*, vol. 4, no. 5, pp. e00390-19, Sep. 2019, doi: 10.1128/mSystems.00390-19.
[58] L. A. Pratt and R. Kolter, “Genetic analysis of Escherichia coli biofilm formation: roles of flagella, motility, chemotaxis and type I pili,” *Molecular Microbiology*, vol. 30, no. 2, pp. 285–293, 1998, doi: 10.1046/j.1365-2958.1998.01061.x.
[59] J. C. Conrad, “Physics of bacterial near-surface motility using flagella and type IV pili: implications for biofilm formation,” *Research in Microbiology*, vol. 163, no. 9, pp. 619–629, Nov. 2012, doi: 10.1016/j.resmic.2012.10.016.
[60] T. K. Wood, A. F. González Barrios, M. Herzberg, and J. Lee, “Motility influences biofilm architecture in Escherichia coli,” *Appl Microbiol Biotechnol*, vol. 72, no. 2, pp. 361–367, Sep. 2006, doi: 10.1007/s00253-005-0263-8.
[61] K. M. Shoemaker and P. H. Moisander, “Seasonal variation in the copepod gut microbiome in the subtropical North Atlantic Ocean,” *Environ Microbiol*, vol. 19, no. 8, pp. 3087–3097, Aug. 2017, doi: 10.1111/1462-2920.13780.
[62] A. Klindworth *et al.*, “Evaluation of general 16S ribosomal RNA gene PCR primers for classical and next-generation sequencing-based diversity studies,” *Nucleic Acids Research*, vol. 41, no. 1, p. e1, Jan. 2013, doi: 10.1093/nar/gks808.
[63] K. M. Shoemaker, S. Duhamel, and P. H. Moisander, “Copepods promote bacterial community changes in surrounding seawater through farming and nutrient enrichment,” *Environ Microbiol*, vol. 21, no. 10, pp. 3737–3750, Oct. 2019, doi: 10.1111/1462-2920.14723.
[64] M. Shangraw and H. Ling, “Separating twin images in digital holographic microscopy using weak scatterers,” *Appl. Opt., AO*, vol. 60, no. 3, pp. 626–634, Jan. 2021, doi: 10.1364/AO.410167.
[65] M. Shangraw and H. Ling, “Improving axial localization of weak phase particles in digital in-line holography,” *Appl. Opt., AO*, vol. 60, no. 24, pp. 7099–7106, Aug. 2021, doi: 10.1364/AO.435021.
[66] J. Katz and J. Sheng, “Applications of Holography in Fluid Mechanics and Particle Dynamics,” *Annual Review of Fluid Mechanics*, vol. 42, no. 1, pp. 531–555, 2010, doi: 10.1146/annurev-fluid-121108-145508.
[67] H. Ling, “Three-dimensional measurement of a particle field using phase retrieval digital holography,” *Appl. Opt., AO*, vol. 59, no. 12, pp. 3551–3559, Apr. 2020, doi: 10.1364/AO.389554.
[68] M. Elius and H. Ling, “Effect of hologram plane position on particle tracking using digital holographic microscopy,” *Appl. Opt., AO*, vol. 61, no. 32, pp. 9415–9422, Nov. 2022, doi: 10.1364/AO.473763.
[69] J. Sheng, E. Malkiel, and J. Katz, “Digital holographic microscope for measuring three-dimensional particle distributions and motions,” *Appl. Opt., AO*, vol. 45, no. 16, pp. 3893–3901, Jun. 2006, doi: 10.1364/AO.45.003893.
[70] N. T. Ouellette, H. Xu, and E. Bodenschatz, “A quantitative study of three-dimensional Lagrangian particle tracking algorithms,” *Exp Fluids*, vol. 40, no. 2, pp. 301–313, Feb. 2006, doi: 10.1007/s00348-005-0068-7.
[71] N. Mordant, A. M. Crawford, and E. Bodenschatz, “Experimental Lagrangian acceleration probability density function measurement,” *Physica D: Nonlinear Phenomena*, vol. 193, no. 1, pp. 245–251, Jun. 2004, doi: 10.1016/j.physd.2004.01.041.
[72] J. L. Nadeau, Y. B. Cho, J. Kühn, and K. Liewer, “Improved Tracking and Resolution of Bacteria in Holographic Microscopy Using Dye and Fluorescent Protein Labeling,” *Frontiers in Chemistry*, vol. 4, 2016, Accessed: Jun. 02, 2023. [Online]. Available: https://www.frontiersin.org/articles/10.3389/fchem.2016.00017

[73] See Supplemental Material at [URL] for Figures S1 to S4.

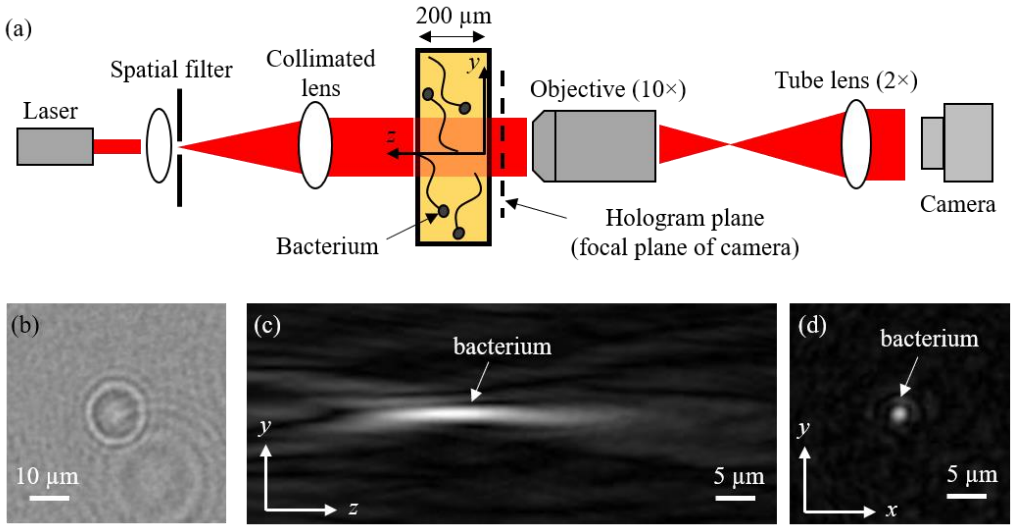

Figure 1. (a) Optical setup of DHM for imaging the 3D motion and growth of bacteria in a closed glass cuvette (the inner walls of the cuvette are located at z=0 and 200 μm, and bacteria are located at $0<z<200$ μm); (b) a sample hologram of one bacteria located at 34 μm away from the hologram plane; (c-d) intensity distributions in the center of the bacteria in y-z plane (c) and x-y plane (d) obtained by reconstruction of the hologram shown in (b).

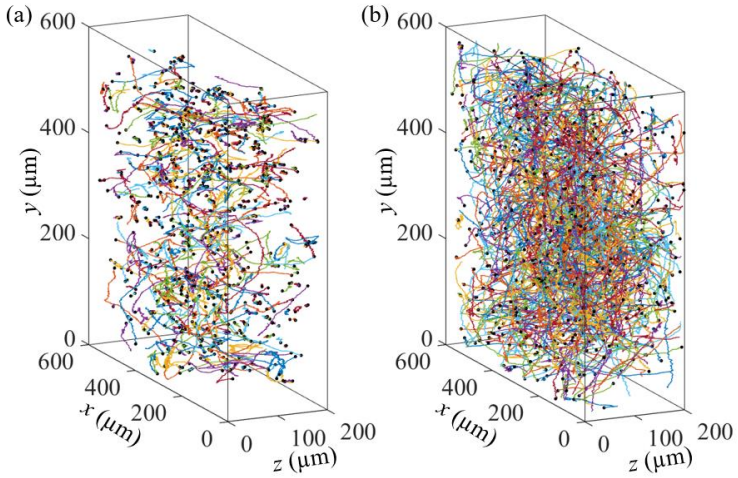

Figure 2. Sample 3D trajectories for UMDC1 (a) and UMDC19 (b) obtained at t=4 hours. The number of trajectories shown in (a) and (b) are 742 and 688 respectively.

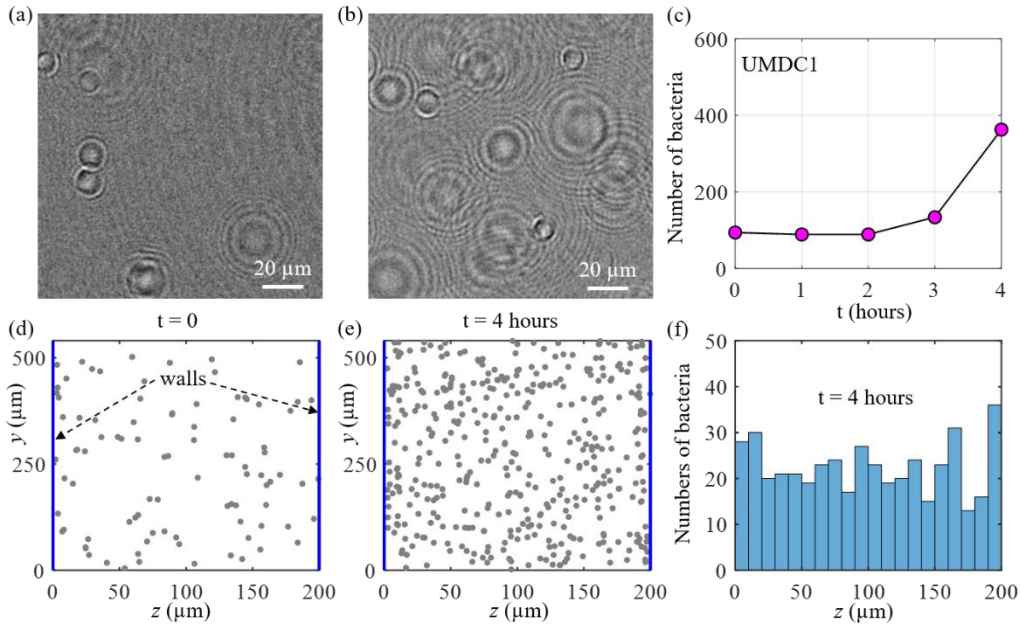

Figure 3. Growth statistics for bacteria UMDC1 with no wall accumulation: (a-b) Sample holograms recorded at the begin (a, t=0) and end (b, t=4 hours) of the experiments (only a small portion of the entire hologram is shown); (c) Number of bacteria as a function of time; (d-e) Spatial distributions of bacteria in the chamber at the begin (d, t=0) and end (e, t=4 hours) of the experiments (the two walls of the chamber are at z=0 and 200 μm); and (f) histogram of bacteria position in *z* direction.

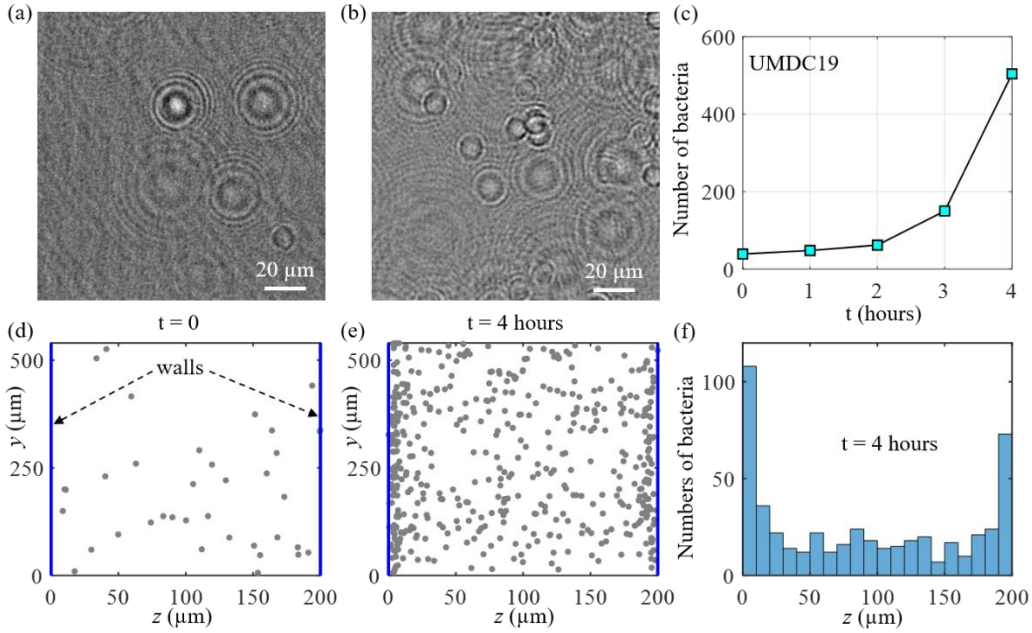

Figure 4. Growth statistics for bacteria UMDC19 with wall accumulation: (a-b) Sample holograms recorded at the begin (a, t=0) and end (b, t=4 hours) of the experiments (only a small portion of the entire hologram is shown); (c) Number of bacteria as a function of time; (d-e) Spatial distributions of bacteria in the chamber at the begin (d, t=0) and end (e, t=4 hours) of the experiments (the two walls of the chamber are at z=0 and 200 μm); and (f) histogram of bacteria position in *z* direction.

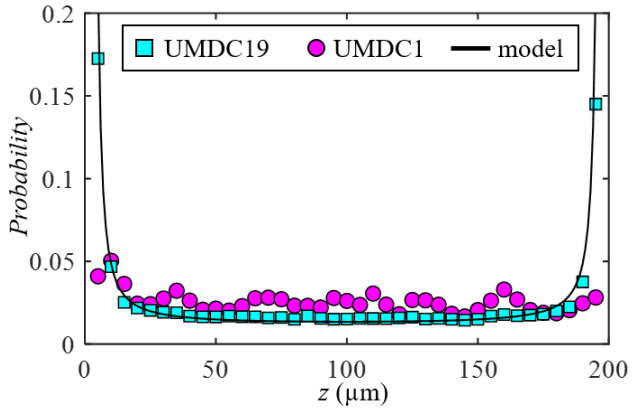

Figure 5. A comparison between the measured density distributions of bacteria and the prediction based on a model proposed by Berke *et al.* [29].

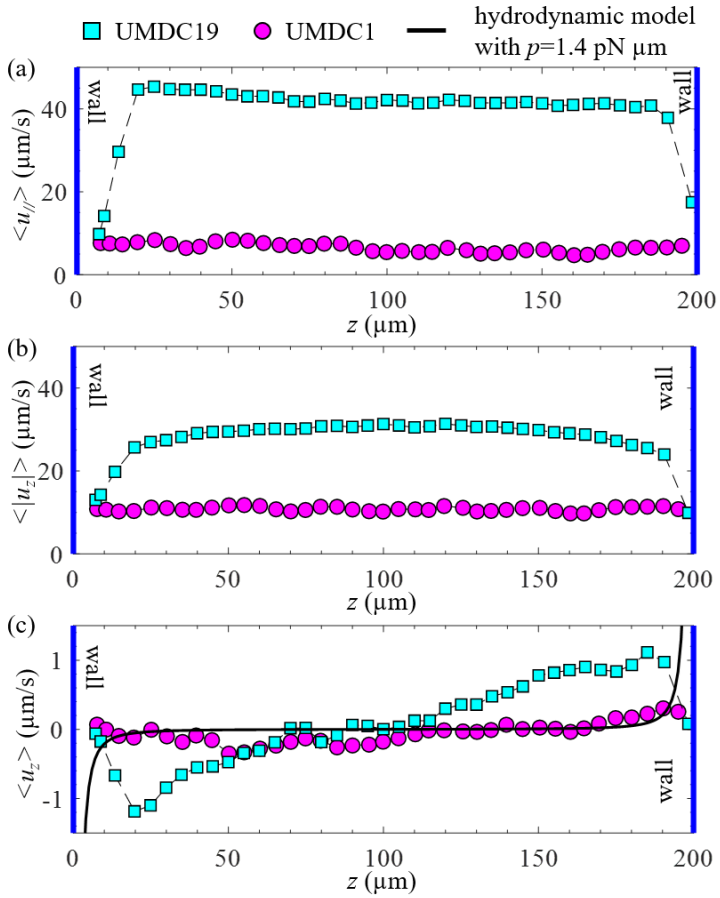

Figure 6. Spatial distributions of velocity as a function z for the two types of bacteria (UMDC1 and UMDC19). (a) $\langle u_{//} \rangle$, (b) $\langle |u_z| \rangle$, and (c) $\langle u_z \rangle$. Results shown are based on the data recorded at t=4 hours. Induced velocity by hydrodynamic interaction with p=1.4 pN μm is also plotted in (c) for comparison.

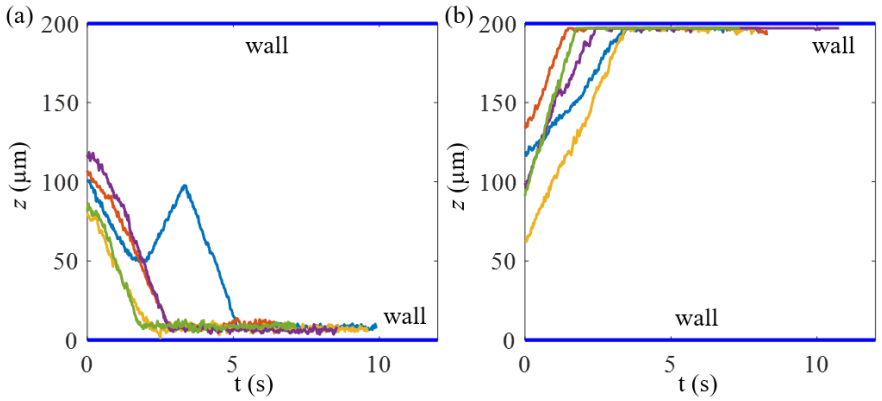

Figure 7. Sample time-variations of z-position of UMDC19 showing cell migration from the bulk region to the walls located at (a) z=0 and (b) z=200 μm.

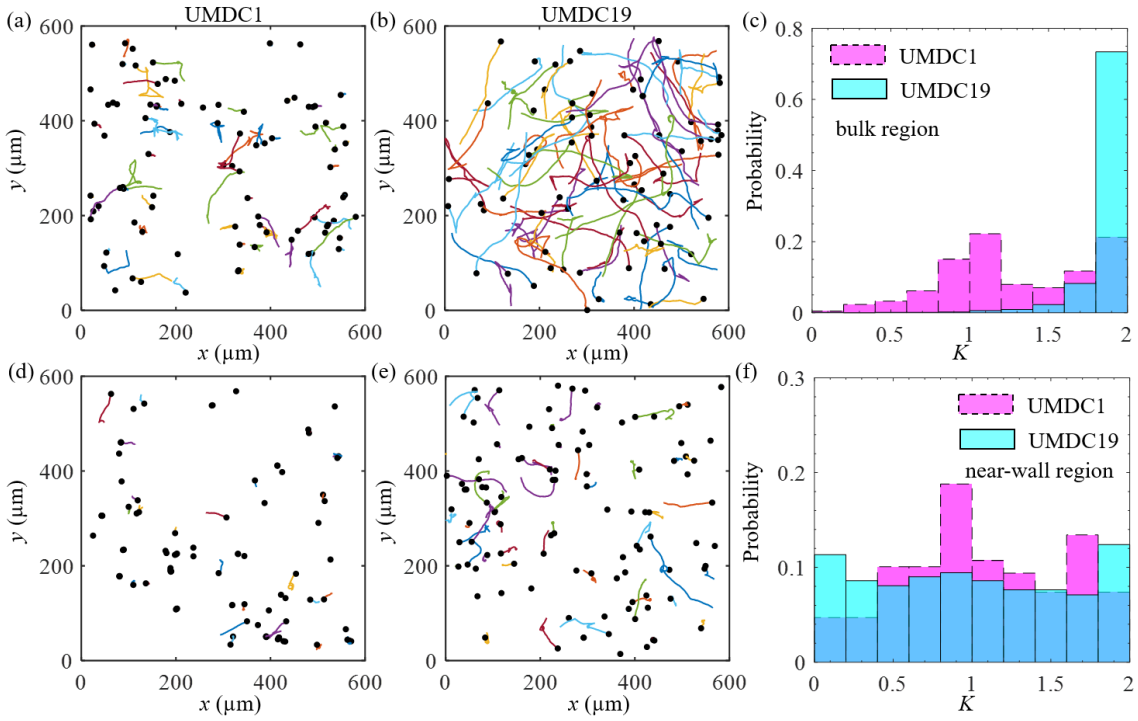

Figure 8. (a-b) Sample movement trajectories of bacteria in the bulk region (50<z<150 μm) (dots denote the position of the bacteria, and lines are the trajectories, all the trajectories are projected to x-y plane); (c) Probability distribution of K for bacteria in the bulk region; (d-e) Sample movement trajectories of bacteria in the near-wall region (0<z<10 μm and 190<z<200 μm); and (f) Probability distribution of K for bacteria in the near-wall region. (a) and (d) correspond to UMDC1. (b) and (e) correspond to UMDC19. Results shown are based on the data recorded at t=4 hours. The numbers of cells in (c) are 1041 for UMDC1 and 1398 for UMDC19. The numbers of cells in (f) are 149 for UMDC1 and 943 for UMDC19.